A Comparative Study of Asymptotically-Optimal Sampling-Based Path Planning Methods

Jazib Ahmad
Department of Computer Science
University of Toronto
jazibahmad@cs.toronto.edu

Jimmy Woo
Department of Computer Science
University of Toronto
jimmywoo@cs.toronto.edu

Sumant Bagri
Department of Computer Science
University of Toronto
sbagri@cs.toronto.edu

Abstract: In this project, we perform a comparative study between three asymptotically-optimal sampling-based path planning algorithms: Fast-marching trees (FMT*), batch informed trees (BIT*), and neural rapidly random-exploring trees (NRRT*). The individual algorithms were be implemented, and their simulated performances in terms of execution time and path costs were observed on environments of various types and complexities. The performance with varying sample counts will was observed, and a qualitative comparison of the optimal paths achieved from each algorithm for a subset of the environments is provided to demonstrate how the planners handle obstacles.

Also talk about results...

Keywords: Sampling-based planning, asymptotically optimal planning

1 Introduction

Path planning is a search problem where the goal is to find a sequence of actions that will lead to an obstacle-free optimal path from a start state to a target state. Grid-based heuristic search algorithms [1] have been proposed in the past that guarantee finding optimal paths that exists. However, these techniques do not scale well to higher dimensional problems as they require discretization of the state space. On the other hand, sampling-based path planning algorithms [2] can solve high-dimensional path planning problems more efficiently. However, these algorithms only converge to optimal paths asymptotically, and in practice may compute sub-optimal paths. Many attempts have been made to make improvements to sampling-based methods [3][4][5], using techniques such as heuristic guided searches, or the reduction of the sampling space. In this project, we implement three sampling-based path planning algorithms, and compare their performances through simulations.

We can formulate the path planning problem by defining the state space and the cost function similar to [2]. Let $\mathcal{X} \in \mathbb{R}^d$, $\mathcal{X}_{free}$, and $\mathcal{X}_{obs}$ be the state space, free space, and the obstacle space respectively where $\mathcal{X}_{obs} \subset \mathcal{X}$ and $\mathcal{X}_{free} = \mathcal{X} \setminus \mathcal{X}_{obs}$. Let $x_{init} \in \mathcal{X}_{free}$, $x_{goal} \in \mathcal{X}_{free}$ be the start and target states respectively. The goal of the path planning problem is to determine a path σ : [0, 1] $\mapsto \mathcal{X}_{free}$ such that $\sigma(0) = x_{init}$, $\sigma(1) = \mathcal{G}(x_{goal})$, where the acceptable goal region is defined as $\mathcal{G}(x_{goal}) = \{x \in \mathcal{X} \,|\, x - x_{goal} < r\}$. Then we can define the path planning problem as minimizing the following cost function:

$$\sigma^* = \underset{\sigma \in \Sigma}{\operatorname{argmin}}\, c(\sigma) \tag{1}$$
$$s.t.\ \sigma(0) = x_{init},\ \sigma(1) = \mathcal{G}(x_{goal}),\ \sigma(t)\ \mathcal{X}_{free},\ \forall t \in [0, 1]$$

where Σ is the set of feasible paths and $c(\sigma)$ is the cost of a single path σ.

2 Related Work

Rapidly random-exploring tree (RRT) [6] is a well studied sampling based algorithm. It utilizes sampling to avoid the discretization of the state space and increase scalability but does not guarantee optimal paths. [2]. Thus many variants have been proposed to improve on its performance by various approaches, heuristic guided searches being a popular method. RRT-Connect [7] builds two RRTs, from both the starting state target state, to advance the trajectory towards each other guided by a heuristic. However, RRT-Connect fails to address the non-optimal path issue. A*-RRT* [8] is another heuristic guided variant, that biases the sampling process using paths generated by A* algorithm [1]. Informed RRT* [3] reduces the number of iterations to convergence from RRT* by reducing the sampling space once a sub-optimal path is found. Similar work has been done to extended the Probabilistic Roadmap algorithm (PRM) as PRM* [2] that converges to an asymptotically optimal solution. However, these approaches do not utilize the ordered search available to grid-based planners. RA* [5] and SBA* [4] directly extend A* to the continuous domain by sampling near heuristically selected vertices of the graph. While these approaches may work efficiently in environments without obstacles, they are susceptible to local minima convergence when faced with obstacles. Diankov and Kuffner [5] address this problem with a minimum allowed distance between vertices, which decreases the possible resolution of the final solution. Persson and Sharf [4] address the problem for SBA* by prioritizing sampling unexplored areas through adding a local sample density to the heuristic for selecting vertices near which to sample. The local sample density must be estimated [9]. In recent years, many attempts have been made to utilize the advancement of deep learning and reinforcement learning methods in sampling-based path planning algorithms. Ichter et al. [10] present method utilizing conditional variational autoencoder (CVAE) to explicitly learn the sampling distribution of the robot state space. Reinforcement learning RRT (RL-RRT) [11] incrementally trains an obstacle-avoiding local planner and a reachability estimator to be used to bias the sample space regions more favourable for optimal paths.

3 Methodology

In this report, we perform a comparison study of three asymptotically-optimal sampling-based path planning algorithms: Fast-marching trees (FMT*) [12], batch informed trees (BIT*), and neural RRT* (NRRT*) [13]. The following section describes the technical details of each of these algorithms, the proposed simulation methods for comparison of planners' performances, as well as the map images used to evaluate the algorithms.

3.1 Fast-Marching Trees

FMT* incorporates the advantages from both single and multiple query sampling-based algorithms in that it eliminates the greediness in RRT* by creating connections nearly optimally instead of trying to find the exactly optimal steering direction. However, in finding the optimal path, it grows a tree (as in the case of RRT*) instead of creating a bi-directional graph employed in the PRM* algorithm.

In the original implementation of FMT*, Janson and Pavone [12] describe the algorithm as an outward growing tree in the cost-to-arrive space which performs a forward-dynamic programming recursion on a fixed sample size. Some of the key features of this algorithm are described below:

- The sample count ($\mathcal{N}$) is fixed and the points are sampled from the free space ($\mathcal{X}_{free}$), beforehand, using a pre-determined distribution. This is described by $\mathcal{M} \subset \mathcal{X}_{free}$
- The tree is built by considering a subset of sampled points that are within the ball $B(\bar{x}, r_n) := \{x \in \mathbb{R}^d : ||x - \bar{x}||_2 < r_n\}$ (i.e "disk-connected"), where r_n is called the *connection radius* and $\bar{x} \in \mathbb{R}^d$ is the query-point
- The algorithm improves in computational complexity by considering a *single*, locally optimal connection, with minimum cost-to-arrive, and adds the connection to the tree only if it

is collision free. If it isnt, however, then the algorithm does not try to find another *"valid"* point in $B(\bar{x}, r_n)$ and simply skips the current query point $\bar{x}$

The basic pseudocode of the FMT* algorithm, as described in [12] is described in Algorithm 1

Algorithm 1 Fast Marching Tree Algorithm (FMT*): Basics

Require: sample set V comprising of x_{init} and n samples in $\mathcal{X}_{free}$, at least one of which is also $\mathcal{X}_{goal}$

Place x_{init} in V_{open} and all other samples in $V_{unvisited}$; initialize tree with root node x_{init}
Find lowest-cost node z in V_{open}
    For each of z's neighbors x in $V_{unvisited}$:
        Find neighbor nodes y V_{open}
        Find locally-optimal one-step connection to x from among nodes y
        If that connection is collision-free, add edge to tree of paths
    Remove successfully connected nodes x from $V_{unvisited}$ and add them to V_{open}
    Remove z from V_{open} and add it to V_{closed}
    Repeat until either:
        (1) V_{open} is empty $\Rightarrow$ report failure
        (2) Lowest-cost node z in V_{open} is in $\mathcal{X}_{goal} \Rightarrow$ return unique path to z and
            report success

Here, $V = \{x_{init}\} \bigcup \mathcal{M}$ and it is partitioned into three different sets: $V_{unvisited}$, V_{open} and V_{closed}. $V_{unvisited}$ contains points that havent been explored yet. V_{open} consists of query-points $\bar{x}$ whose cost-to-arrive from x_{init} has been determined and are active for making new connections (i.e. tree-leaves). V_{closed} consists of points which have been explored and are no-longer considered for new connections (i.e. parent nodes in the tree).

The *connection radius*, r_n, is computed as follows ([12]),

$$r_n = \gamma \left(\frac{\log(\mathcal{N})}{\mathcal{N}} \right)^{1/d}$$

$$\text{where, } \gamma > 2 \left(\frac{\mu(\mathcal{X}_{free})}{d \times \zeta_d} \right)^{1/d} \text{ and } d \text{ is the dimensionality}$$

Here, $\mu(\mathcal{X}_{free})$ is the Lebesgue-measure of the free space and ζ_d is the volume of a unit-ball in d-dimensional Euclidean space

In our implementation of FMT*, we have made two notable modifications

First, We have added euclidean-heuristics (with weight$= 1.0$) to the computation for cost-to-arrive at node x in $V_{unvisited}$ from x_{init} via a node y in V_{open}. This is defined, mathematically, below:

$$c(x) = ||x - y||_2 + 1.0 \times (||x - x_{goal}||_2 - ||y - x_{goal}||)$$

Second, We maintain the obstacle nodes as a KDTree for faster query when checking for collisions

We define the pseudocode for performing collision checks in FMT* in Algorithm. 2

The performance benefits of FMT* are observed in higher dimensions (e.g. 6DoF Robotic Manipulators) where performing collision-checks is costly.

3.2 Batch Informed Trees

BIT* constructs an implicit Randomly Generated Graph (RGG) and an explicit spanning tree by sampling and processing batches of states [9]. The sampled states define an RGG with implicit edges, while a spanning tree with explicit edges is created outward from the starting state towards

Algorithm 2 Algorithm for Collision Checks

Require: obstacles stored as a KDTree. dCol defining the collision clearance
Input: start, target($\leftarrow \emptyset$) ▷ check for collisions between start and target
Output: *bool* ▷ True if collision-free, else false
function COLLISIONFREE(start, target)
  if target$\leftarrow \emptyset$ or start = target **then**
    return NEAR(obstacles,start,1) $>$ dCol
  end if
  $\overline{ts} \longleftarrow \frac{\overline{target}-\overline{start}}{||\overline{target}-\overline{start}||_2}$ ▷ vector from start to target
  pts $\longleftarrow (\overline{start}, 0.1 \times \overline{ts}, \cdots, \overline{target})$ ▷ segmenting the connecting line
  return $\min$[NEAR(obstacles,pts,1)] $>$ dCol
end function

the goal state. Before a solution is found, the states are sampled uniformly from $\mathcal{X}_{free}$. However, once a solution has been found, the states are sampled only from the space that may improve the existing solution. The processing of these states occurs in an order of increasing estimated solution cost, as determined by the heuristic. An edge between the existing state on the spanning tree and a free state on the RGG is created if it is collision free and the estimated cost from the starting state through that edge and to the goal is lower than the current solution cost. If the spanning tree can no longer be expanded or a new solution is found, a new batch is sampled and the process repeats. Because of processing multiple batches of samples in this way, BIT* has anytime resolution. This means that it can find a sub-optimal solution quickly with only a few iterations. As the number of iterations increases, it samples more batches, and can use the sub-optimal solution to converge asymptotically towards the optimal solution. The complete algorithm is defined formally in [9].

Algorithm 3 BIT*

V $\leftarrow\{\mathrm{x}_{init}\}$; E $\leftarrow \emptyset$; $\mathrm{X}_{samples} \leftarrow\{\mathrm{x}_{goal}\}$ repeat: r $\in$ (1, 2, ..., $\mathcal{R}$) Generate trajectory τ from policy $\pi_k^{(r)}$ Perform behavioral cloning on τ to obtain policy $\pi_{BC}^{(k,r)}$ $\epsilon \in \mathcal{E}$ Generate a set of $\mathcal{N}$ trajectories according to $\pi_{BC}^{k,r}(\cdot|\epsilon)$ Generate automatic preference labels $\tau_i \succ \tau_j$: $\tau_i \sim \pi_{BC}^{(k,r)}(\cdot|\epsilon_i), \tau_j \sim \pi_{BC}^{(k,r)}(\cdot|\epsilon_j), \epsilon_i < \epsilon_j$ and augment $\mathcal{T}$ Run T-REX on $\mathcal{T}$ to obtain reward function estimate $\hat{R}$ Obtain policies $\pi_{k+1}^{(1)}$, $\pi_{k+1}^{(2)}$..., $\pi_{k+1}^{(\mathcal{R})}$ through reinforcement learning with reward $\hat{R}$ Return $\pi_{\mathcal{K}}^{(1)}$, ..., $\pi_{\mathcal{K}}^{(\mathcal{R})}$

3.3 Neural RRT*

Neural RRT* is a non-uniform sampling-based path planning algorithm that aims to take advantage of the optimal path costs of the A* algorithm as well as the asymptotic optimality of the RRT* algorithm. Instead of sampling from the state space using just a uniform distribution, a non-uniform distribution learned by a convolutional neural network (CNN) trained on optimal paths generated from the A* algorithm is used to achieve non-uniform sampling. Unlike many of the RRT variant algorithms, the NRRT* algorithm does not depend on any human-designed heuristics to improve its performance. It also maintains the probabilistic completeness and the asymptotic optimality of the RRT* algorithm. Through simulations, it has been shown to perform superior compared to RRT* and IRRT* [13]. The following section will cover the overview of the NRRT* algorithm, the model architecture of the CNN, the data generation process, and the training process of the CNN.

3.3.1 Overview of NRRT* Algorithm

The NRRT* algorithm is an extension of RRT* that provides an efficient non-uniform sampling scheme. The steps of the NRRT* algorithm are shown in Algorithm 4: The NRRT* algorithm builds upon RRT* and utilizes both $ChooseParent$ and $Rewire$ to achieve asymptotic optimality, but includes an additional non-uniform sampling method. If $Rand() > \alpha = 0.5$, a state is sampled

Algorithm 4 NRRT*

Input: x_{init} $\mathcal{G}(x_{goal}), Map, S, C$ **Output:** $\mathcal{T}$ V $\leftarrow x_{init}$; $E \leftarrow \emptyset$; $\mathcal{T} = (V, E)$ $\mathcal{O} \leftarrow (Map, S, C)$ i = 1, ..., N $Rand() > 0.5$ $x_{rand} \leftarrow$ NonuniformSample($\mathcal{O}$); $x_{rand} \leftarrow$ UniformSample(); $x_{rand} \leftarrow$ UniformSample(); $x_{nearest} \leftarrow$ Nearest($\mathcal{T}, x_{rand}$); $x_{new} \leftarrow$ Steer($x_{nearest}, x_{rand}$); $ObstacleFree(x_{nearest}, x_{rand})$ $\mathcal{T} \leftarrow$ Extend($\mathcal{T}, x_{new}$); Rewire(); $x_{new} \in \mathcal{G}(x_{goal})$ Return($\mathcal{T}$); Return $failure$;

using the probability distribution generated from the CNN. Otherwise, the procedure follows RRT*. In fact, NRRT* will perform identical to RRT* if $\alpha = 0$. Wang et al. [13] state that the probabilistic distribution generated from the CNN is not always a continuous path from the start state to the target state, and thus uniform sampling is required to guarantee convergence. The authors also present that $\alpha = 0.5$ offers the best balance between performance and ensuring full coverage of the environment.

3.3.2 CNN Model

The CNN model uses two ResNet50 (*conv2_x* and *conv4_x* layers)[14] based encoders to generate a high-level image feature map, and a low-level image feature map from the input RGB image. The network also takes two robotic attributes, stepsize and obstacle clearance, as inputs to two fully connected layers. The output of these layers are repeated width and length wise to match the final dimensions of the image feature maps. After applying atrous spatial pyramid pooling (ASPP) [15], the low-level and high-level image feature maps are concatenated with the low-level and high-level attribute feature maps respectively. The resulting high-level feature map is linearly resized, and concatenated with the resulting low-level feature map to complete the encoding process. As the decoder architecture was not presented in the original paper, a U-Net based decoder was implemented, with 3 decoding blocks each consisting of a tranpose convolutional layer followed by two convolutional layers. The resulting network is fully convolutional, allowing varying image resolutions. Refer to Figure 1 for an overview of the cnn architecture [13].

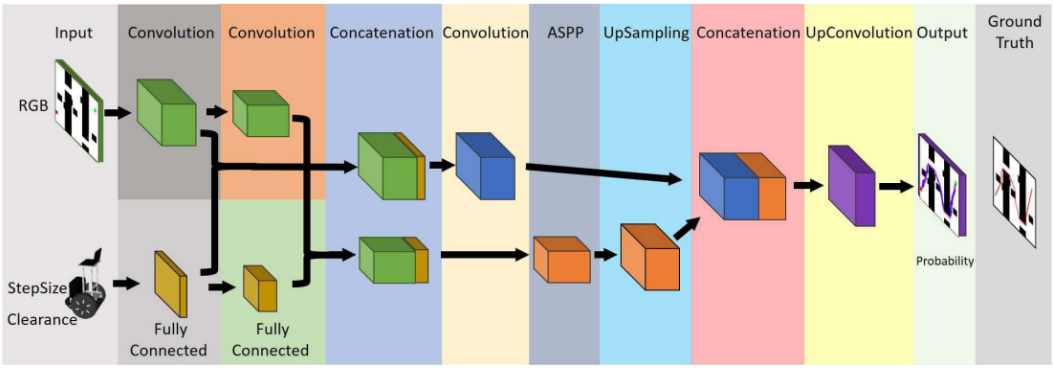

Figure 1: Architecture of CNN model for NRRT*

To generate the training data, start states and target states were randomly selected from a randomly selected subset of 5547 201 x 201 image dataset, resulting in 26960 combinations of start and target states with their corresponding optimal paths generated by running the A* algorithm. The optimal paths were converted to ground truth binary labels by assigning each pixel a value of 0 or 1, 0 for states not included in the optimal path, and 1 for pixels residing on the optimal path found by the A* algorithm. The same map image dataset was used for the simulations, refer to Section **??** for additional details on the dataset. To train the CNN model, we assign individual pixels of the training images with pixel values from 0 to 3, where 0 represents a free state, 1 represents a state occupied by an obstacle, and 2 and 3 represent the start and target states respectively. The loss function is

defined as:

$$L = \sum ce(\mathcal{O}, \mathcal{G}) \tag{2}$$

where $\mathcal{O}$ is the output of the network, $\mathcal{G}$ is the ground truth label, and L is the sum of cross-entropy loss across all training observations. As per the instructions of [13], Adam optimizer with ϵ = 1e-4, β_1 = 0.9, and β_2 = 0.999 was used for the training process, while using a reduced batch size of 10 due to hardware limitations.

3.4 Description of the Simulation Process

The dataset [16] used for the simulation based evaluation of the three algorithms consists of 7 images from 7 distinct categories: alternating gaps, bugtrap forest, forest gaps and forest, mazes, single bugtraps, and multiple bugtraps. The images and their corresponding start/target state combinatinos is displayed in Figure 2.

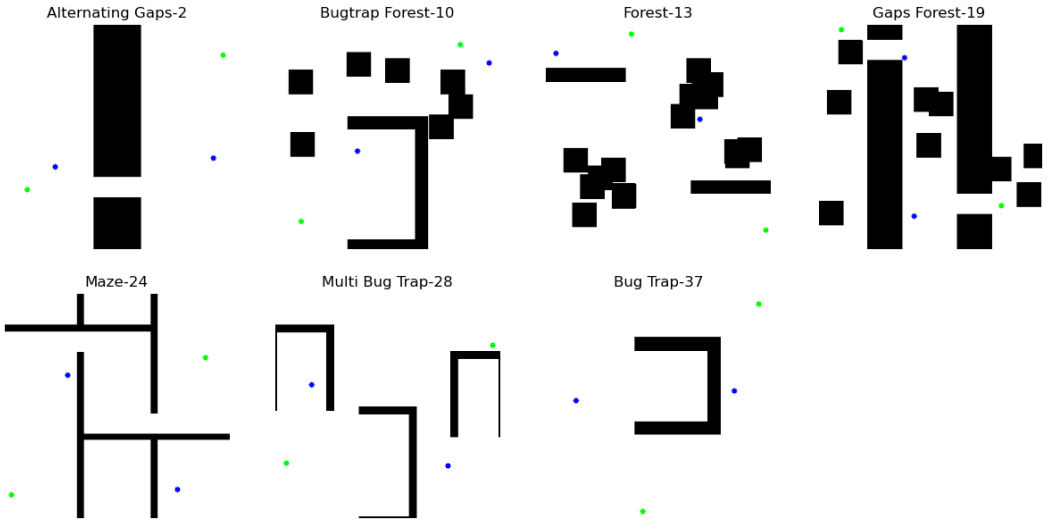

Figure 2: Map images used for simulations, start/target states paired by same color

All start/target pairs have a reachable path with the exception of one pair in *Maze-24*, and most start/target pairs are blocked by one or more obstacles, and are not directly reachable. To observe the variation in execution time, calculated path cost, and success rate of the three algorithms in various scenarios with statistical significance, each algorithm will execute its path planning 5 times per state/target combination, for two state/target combinations on 7 maps, with 9 different batch sizes for sampling ([5, 10, 20, 40, 80, 100, 300, 600, 1000]), resulting in a total of 630 runs per each algorithm. The resulting metrics (further discussed in 4) will be plotted grouped by map type and state/target pair to observe their respective patterns

4 Evaluation

This section is structured as follows: First, we mathematically define the different path-planning metrics used in the evaluation scheme. Then, we compare the performance of algorithms based on these metrics (using trend-plots generated from the simulations) to understand their behaviour in different situations. We describe a few, specific, state-space scenarios as well as some algorithmic factors and discuss their effects on the different metrics. Finally, we provide a qualitative comparison for the different paths generated by the algorithms for a specific subset of the maps and states.

4.1 Defining the Metrics

4.1.1 Solution Cost ($\mathcal{J}$)

The solution cost, $\mathcal{J}$, is defined as the cost-to-come to the goal location (`goal`) from the start location (`start`) along the path defined by the path-planning algorithm. We evaluate the cost ($\mathcal{J}$) as follows: For a set of N nodes in the free space $\mathcal{X}_{free}$, let $\mathcal{P} \subset \mathcal{X}_{free}$ be the set of nodes along the optimal path as computed by the path planning algorithm $\{\mathcal{X}_{free}, x_{init}, \mathcal{G}(x_{goal})\}$; Then the cost $\mathcal{J}$ is defined as:

$$\mathcal{J} = \sum_{i=1}^{N} ||x_i - Parent(x_i)||_2, \text{ where } x_i \in \mathcal{P} \tag{3}$$

4.1.2 Execution Time ($\mathcal{T}$)

We evaluate the execution time, $\mathcal{T}$, as follows: Let, τ_{fmt}, τ_{bit} and τ_{nrrt} denote the time-per-iteration for the FMT*, BIT* and NRRT* algorithms respectively. Let, n_{fmt} and n_{nrrt} denote the number of iterations performed by FMT* and NRRT*, respectively, before they find a solution. Also, we cap the maximum number of iterations that can be performed by each algorithm with a common value. Let this be n_max. Then the execution time $\mathcal{T}$ is defined as:

$$\text{FMT*}, \quad \mathcal{T}_{fmt} = \min(n_{fmt}, n\_max) \times \tau_{fmt} \tag{4}$$

$$\text{NRRT*}, \quad \mathcal{T}_{nrrt} = \min(n_{nrrt}, n\_max) \times \tau_{nrrt} \tag{5}$$

$$\text{BIT*}, \quad \mathcal{T}_{bit} = \begin{cases} \tau_{bit} & \text{if } \mathcal{J}_{bit} = ||\texttt{start} - \texttt{goal}||_2 \\ n\_max \times \tau_{bit} & \text{otherwise} \end{cases} \tag{6}$$

Due to the anytime resolution of BIT*, its execution time is recorded differently then FMT* and NRRT*. For FMT* and NRRT*, the final execution time it takes for the algorithm to find any feasible solution from `start` to `goal` is recorded. For BIT*, the execution time is recorded on each iteration of the algorithm.

4.1.3 Success Rate ($\mathcal{Q}$)

For sampling based algorithms, the random sampling of potential nodes in the graph/tree introduces an additional "uncertainty" (alongwith the feasibility) in the ability of the algorithm to find any feasible solution. This uncertainty can be modeled as the entropy precipitating from the probabilistic distribution used for the random-sampling.

Therefore, it is important to quantify the tolerance of an algorithm to this uncertainty. We achieve this by computing the success rate for each algorithm over N runs - on the same map with the same `start` and `goal` states - using a different seed values for the random-generator function in each run. The success rate, for a specific map with fixed `start` and `goal` states, is defined as:

$$\mathcal{Q} = \frac{\sum_{i=1}^{N} \mathbb{1}(\texttt{hasPath[start, goal]} = True)}{N} \tag{7}$$

where, `hasPath[start, goal]` returns $True$ if the algorithm is able to find a path from `start` to `goal`. We have used $N = 5$ for our simulations.

4.1.4 Sample Count ($\mathcal{N}$)

Sample count is defined differently for FMT* and BIT*/NRRT*. For FMT*, the sample count is fixed before the algorithm begins finding a path. However, both BIT* and NRRT* perform sampling in batches. Therefore, the final sample count for BIT* and NRRT* depends on the number of

iterations the algorithm performs. For BIT*, a cumulative value of the number of points sampled in each batch is recorded.

For, FMT*, we have used the following sample counts: $[5, 10, 20, 40, 80, 100, 300, 600, 1000]$

(PLEASE ELABORATE A BIT MORE ON HOW THE SAMPLING IS DONE FOR BIT* AND NRRT*)

4.1.5 Number of collision checks ($\mathcal{C}$)

This is defined as the total number of calls each algorithm makes to `CheckCollision` before adding a node to the graph/tree. (Refer each algorithm's methodology for performing the collision check as defined in 3)

4.2 Performance Analysis: Metric evaluation

4.2.1 Solution Cost ($\mathcal{J}$) vs Execution Time ($\mathcal{T}$) (refer Fig. 3)

BIT* shows the best performance in most cases with a faster convergence rate to a more optimal solution as it achieves the lowest solution cost in most cases. It is also observed that in some cases the solution cost for BIT* remains constant over a certain number of iterations but drops to a lower solution cost with sufficiently large number of iterations.

FMT* with euclidean-heuristics always performs much better than the standard FMT* as expected. FMT* with heuristics also seems to perform better than NRRT* in most cases. Generally, the solution cost decreases with increasing execution time.

4.2.2 Success Rate ($\mathcal{Q}$) vs Execution Time ($\mathcal{T}$) (refer Fig. 4)

All algorithms reach $\mathcal{Q} = 1.0(\hat{\mathcal{Q}})$ within 5 seconds of execution for almost all the map environments. Only in the case of Maze and Gaps Forest, FMT* takes much longer to achieve $\hat{\mathcal{Q}}$. BIT* is the fastest in achieving $\hat{\mathcal{Q}}$ with the other algorithms showing only a marginally slower convergence in most map environments. FMT* without heuristcs is the slowest to converge in all scenarios

4.2.3 Success Rate ($\mathcal{Q}$) vs Sample Count ($\mathcal{N}$) (refer Fig. 5)

For BugTrap and Forest (simple environments), FMT* requires a relatively smaller sample count ($\sim$ 80) to achieve $\hat{\mathcal{Q}}$. However, for more complex enviroments such as BugTrap-Forest, Gaps-Forest, Maze and Multi-BugTrap, BIT* achieves $\hat{\mathcal{Q}}$ most efficiently.

A noteworthy point about BIT* is that it is able to achieve $\hat{\mathcal{Q}}$ with almost the same sample count ($\sim$ 100) in all map environments. NRRT* seems to require a relatively larger sample count to achieve $\hat{\mathcal{Q}}$ in most map environments.

4.2.4 Sample Count ($\mathcal{N}$) vs Number of collision checks ($\mathcal{C}$) (refer Fig. 6)

In this analysis, it is clearly observed that FMT* performs significantly fewer collision checks compared to BIT*. FMT* with euclidean-heuristics performs the least number of collision checks. FMT* performs the maximum number of collision checks for the maze environment. The significantly lower number of collision checks for FMT* is due to its "lazy collision checking" behavior which is what makes it perform better in high dimensional environments.

4.3 Qualitative Analysis: Generated Paths

FMT*:

FMT* progressively improves on the optimality of the path found as the sample count is increased. This can be observed from the paths generated by FMT* for the Maze environment with increasing sample count as shown in Fig. 8

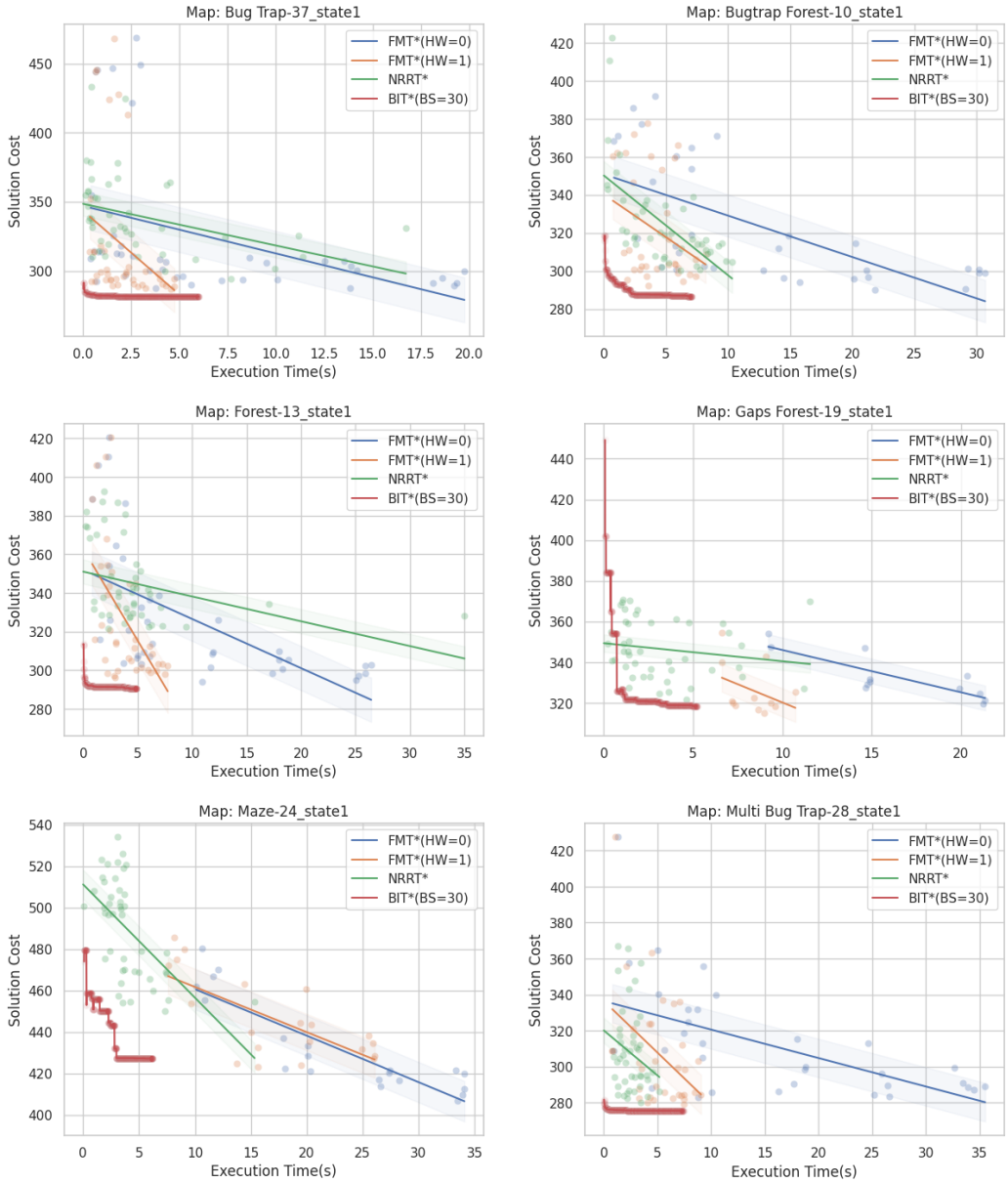

Figure 3: Comparing solution cost with runtime for FMT* without heuristics (blue), FMT* with euclidean-heuristics (weigth=1.0) (orange), BIT* with batch-size=30 (red) and NRRT* (green) in different map environments

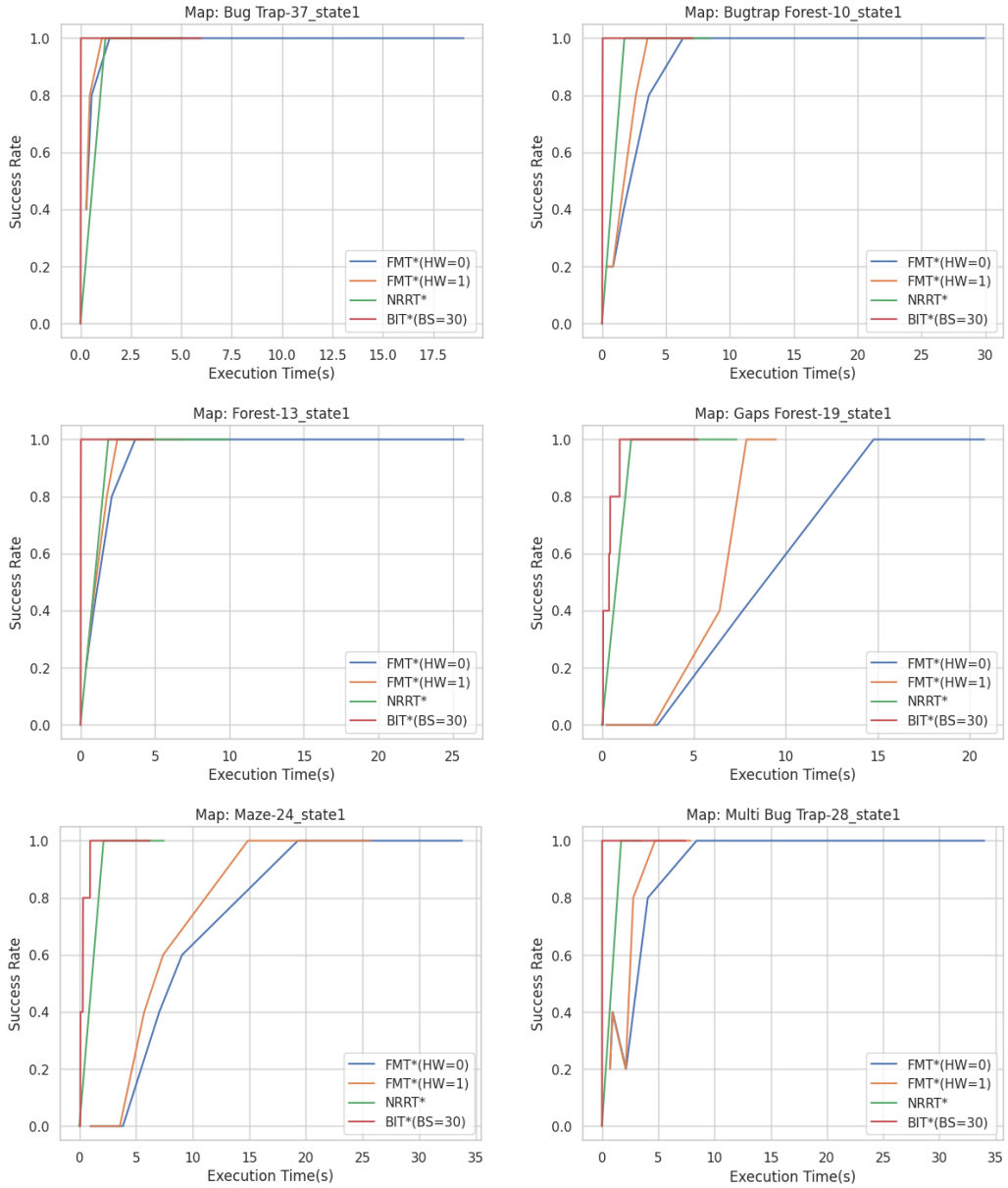

Figure 4: Comparing success rate with runtime for FMT* without heuristics (blue), FMT* with euclidean-heuristics (weigth=1.0) (orange), BIT* with batch-size=30 (red) and NRRT* (green) in different map environments

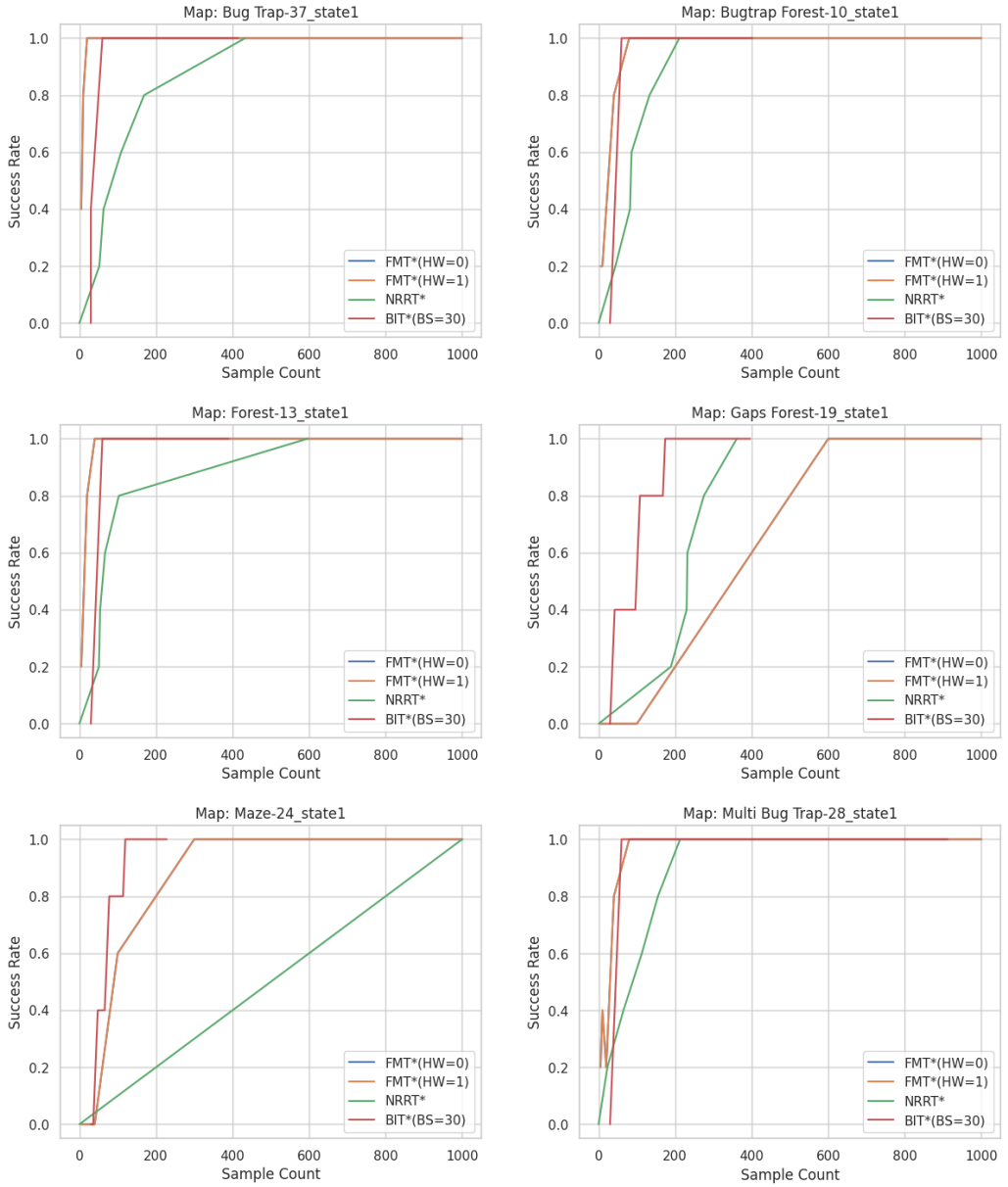

Figure 5: Comparing success rate with sample count for FMT* without heuristics (blue), FMT* with euclidean-heuristics (weigth=1.0) (orange), BIT* with batch-size=30 (red) and NRRT* (green) in different map environments

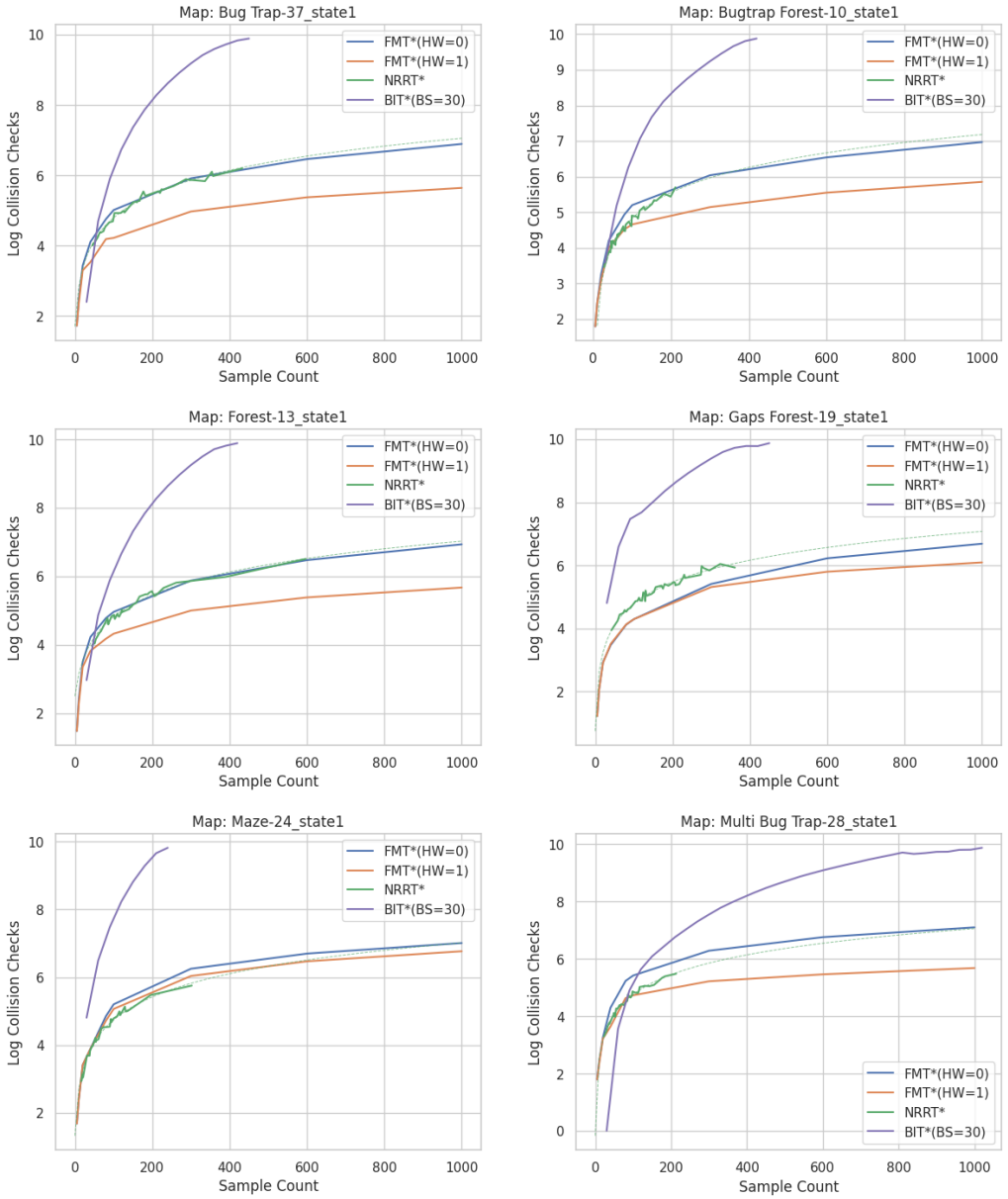

Figure 6: Comparing sample count with number of collision checks made by FMT* without heuristics (blue), FMT* with euclidean-heuristics (weigth=1.0) (orange), BIT* with batch-size=30 (red) and NRRT* (green) in different map environments

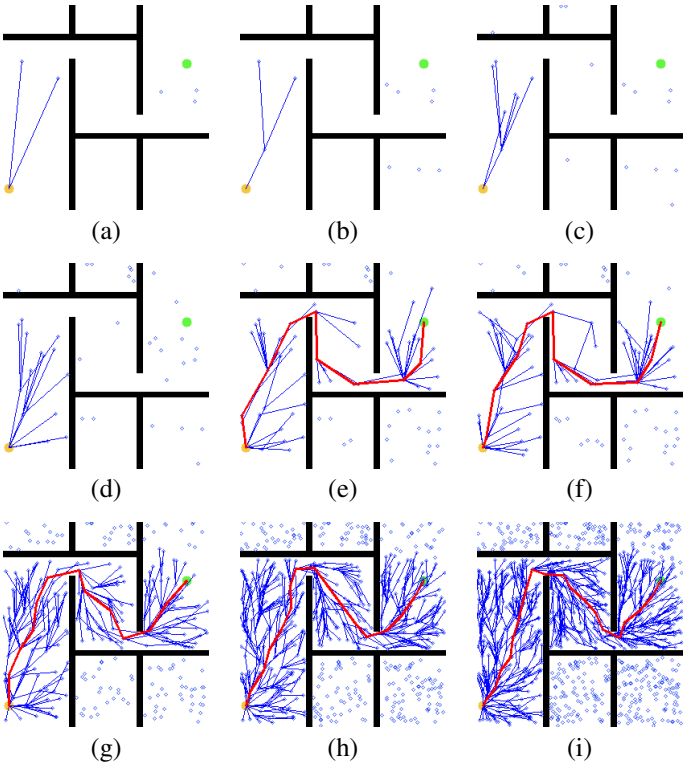

Figure 7: Paths generated by FMT* (without heuristics) for the maze environment with increasing sample count: (a)-5, (b)-10, (c)-20, (d)-40, (e)-80, (f)-100, (g)-300, (h)-600, (i)-1000. Red line indicates the final path generated by the algorithm

As the sample count increases, the algorithm is able to avoid unnecessary turns to generate a path with longer linear-subpaths thus minimizing the cost.

An additional set of simulations were performed for FMT* specifically which incorporates euclidean-heuristics (as described in 3.1). The paths generated by each FMT* algorithm on the Forest map is described in Fig **??**.

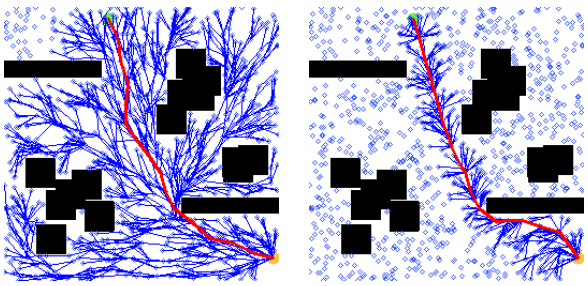

Figure 8: Paths generated by FMT* on the Forest map: (a)- without heuristics and (b) - with euclidean-heuristics (weight=1.0). Red line indicates the final path generated by the algorithm. Blue lines indicate the nodes visited by the algorithm

FMT* with euclidean-heuristics visits fewer nodes while searching for a path and is thus able to converge faster. Since we use euclidean-heuristics with a euclidean cost-to-come to pick the next

node in the tree, FMT* with heuristics is able to generate a more optimal path than the standard FMT* algorithm.

BIT*:

The final paths produced by BIT* were mostly identical, with only a few minor differences. The reason for the similarity is that the maximum number of iterations was set to a large value, allowing all runs to converge closer to the optimal path. Still, the differences were more noticeable for more complicated environments. Figure 9 shows a highlight of some of the paths produced by the algorithm. In case of the existence of the minor differences, the better paths have been selected. These images show some of the characteristics of BIT*. For example, they show a higher sampling density in some regions. That is because BIT* samples in the region that contains a more optimal path than the current solution. This is most obvious in Fig 9 (g). However, it seems to be an ineffective strategy for the maze in Fig 9 (e). The images also show that the spanning tree in BIT* is constructed starting from the `start` state, as seen from the density of the blue lines. Finally, the images demonstrate the ability of BIT* to find a path through relatively narrow openings, as seen best in Fig 9 (d).

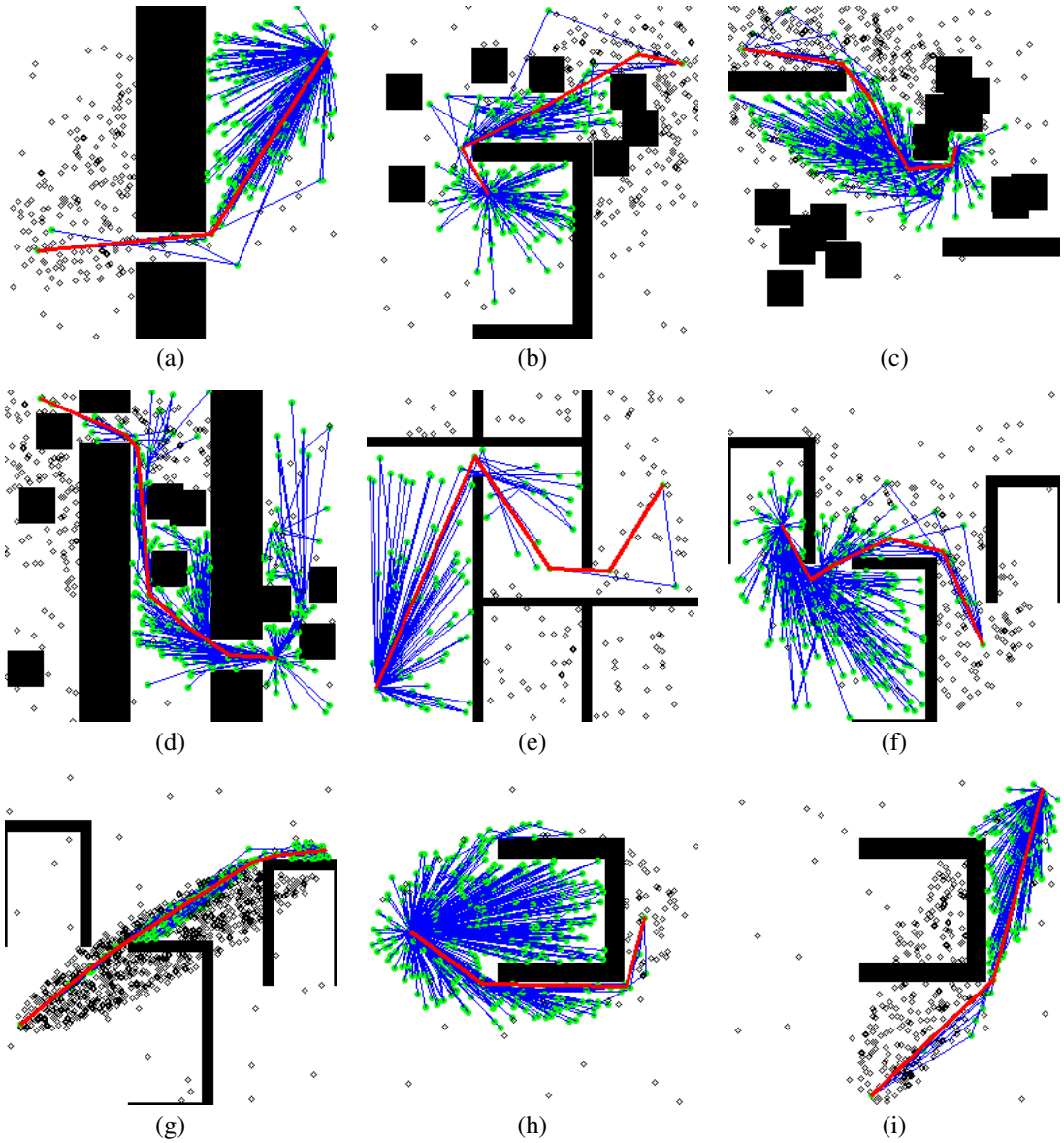

Figure 9: Paths generated by BIT* (Batch Size=30)) for various maze environments. Red line indicates the final path generated by the algorithm

NRRT*:

It is evident from the generated paths, distribution of the non-uniform sampling space, and the nodes explored that the CNN did not adequately estimate the probability distribution corresponding to optimal paths generated by the A* algorithm. It is evident from visual inspection of Figure 10 that the computed path is sub-optimal. The explored nodes and their corresponding paths are extending outwards in a straight manner, similar to the paths generated from RRT* due to the rewiring procedure. The fact that the plot paths closely resembles paths generated from RRT* is an indication that even with the sampling rate $\alpha = 0.5$, the non-uniform sampling is not contributing much in the exploration of the state space. When observing the distribution plot, it is evident that pixels with high probabilities of being on the optimal path do not correspond to the pixels associated with the actual optimal path. Furthermore, a non-negligible amount of the pixels identified as optimal lie on obstacles, meaning sampling from these regions will increment the algorithm iterations and collision check count with no improvements to the path planning task. Further discussions on the

discrepencies between the reported results in [13] and the experimentally obtained results can be found in Section 5.1.

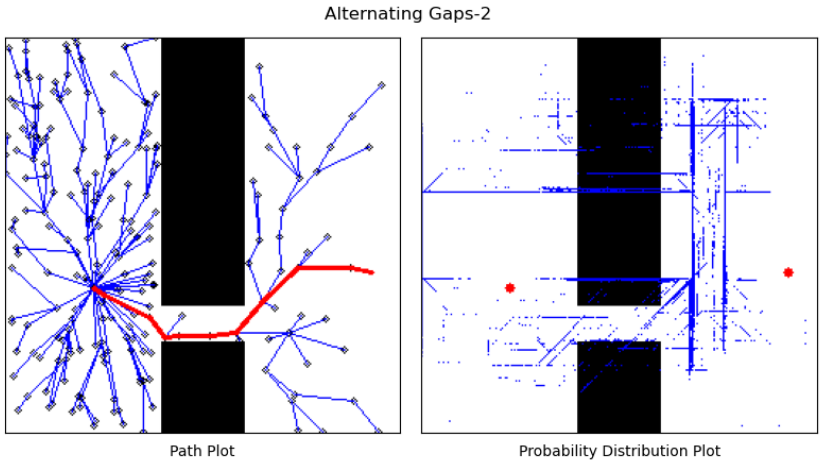

Figure 10: Path plot and sampling distribution plot of Alternating Gaps-2; Blue indicates $p(optimal) > 0.5$ in the distribution plot

4.4 Analyzing edge-cases: State Specific Configurations

4.4.1 Straight line paths

In one of the simulations run on the Gaps-Forest map, the path from `start` to `goal` was a straight line with no obstacles along this line. In this section, we qualitatively compare the paths generated by each algorithm in such a scenario

FMT*:

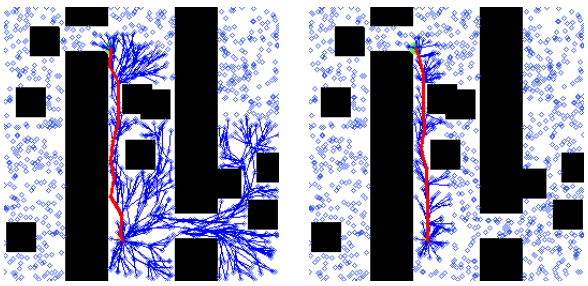

(a) (b)

Figure 11: Paths generated by FMT* on the Gaps-Forest map: (a)- without heuristics and (b) - with euclidean-heuristics (weight=1.0). Red line indicates the final path generated by the algorithm. Blue lines indicate the nodes visited by the algorithm

BIT*:

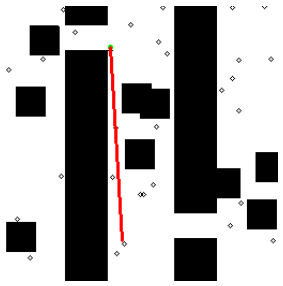

Figure 12: Path generated by BIT* on the Gaps-Forest map. Red line indicates the final path generated by the algorithm.

NRRT*:

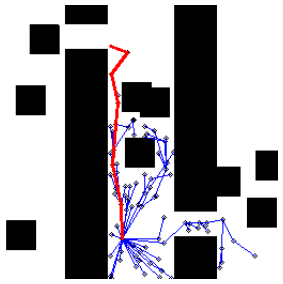

Figure 13: Path generated by NRRT* on the Gaps-Forest map. Red line indicates the final path generated by the algorithm.

4.4.2 Unreachable goals

Often times, there are cases where the goal is unreachable from the start location on the map. We outline one such case that we encountered during our simulations for the Maze environment where the goal was entirely enclosed by obstacles. In such situations, it is important to evaluate how fast can the algorithm can report "no-solution". This can be evaluated using two metrics: Mean execution time per sample count and Mean number of collision check per sample count. We compute and report these metrics for the three algorithms in Table. 1.

Table 1: Running FMT*, BIT* and NRRT* on a map with an unreachable goal

Alg.	Mean execution time per sample count	Mean no. collision checks per sample count
FMT*	0.082	1.48
FMT* (with heuristics)	0.080	1.48
BIT*	0.021	63.25
NRRT*	0.026	1.19

5 Limitations

5.1 NRRT* CNN

6 Conclusion

We presented a comparison...

Acknowledgements

iD-REX was implemented by extensively modifying the original code for D-REX by Brown et al. accompanying Assignment 2. The code for D-REX is publicly available on Github.

References

[1] P. E. Hart, N. J. Nilsson, and B. Raphael. A formal basis for the heuristic determination of minimum cost paths. *IEEE Transactions on Systems Science and Cybernetics*, 4(2):100–107, 1968. doi:10.1109/TSSC.1968.300136.

[2] S. Karaman and E. Frazzoli. Sampling-based algorithms for optimal motion planning. *CoRR*, abs/1105.1186, 2011.

[3] J. D. Gammell, S. S. Srinivasa, and T. D. Barfoot. Informed rrt: Optimal sampling-based path planning focused via direct sampling of an admissible ellipsoidal heuristic. In *2014 IEEE/RSJ International Conference on Intelligent Robots and Systems*, pages 2997–3004, 2014. doi:10.1109/IROS.2014.6942976.

[4] S. M. Persson and I. Sharf. Sampling-based a* algorithm for robot path-planning. *The International Journal of Robotics Research*, 33(13):1683–1708, 2014.

[5] R. Diankov and J. Kuffner. Randomized statistical path planning. In *2007 IEEE/RSJ International Conference on Intelligent Robots and Systems*, pages 1–6, 10 2007. doi:10.1109/IROS.2007.4399557.

[6] S. M. LaValle. Rapidly-exploring random trees : a new tool for path planning. *The annual research report*, 1998.

[7] J. Kuffner and S. LaValle. Rrt-connect: An efficient approach to single-query path planning. In *Proceedings 2000 ICRA. Millennium Conference. IEEE International Conference on Robotics and Automation. Symposia Proceedings (Cat. No.00CH37065)*, volume 2, pages 995–1001 vol.2, 2000. doi:10.1109/ROBOT.2000.844730.

[8] M. Brunner, B. Brüggemann, and D. Schulz. Hierarchical rough terrain motion planning using an optimal sampling-based method. In *2013 IEEE International Conference on Robotics and Automation*, pages 5539–5544, 2013. doi:10.1109/ICRA.2013.6631372.

[9] J. D. Gammell, S. S. Srinivasa, and T. D. Barfoot. Bit*: Batch informed trees for optimal sampling-based planning via dynamic programming on implicit random geometric graphs. *CoRR*, abs/1405.5848, 2014.

[10] B. Ichter, J. Harrison, and M. Pavone. Learning sampling distributions for robot motion planning, 2017. URL `https://arxiv.org/abs/1709.05448`.

[11] H.-T. L. Chiang, J. Hsu, M. Fiser, L. Tapia, and A. Faust. Rl-rrt: Kinodynamic motion planning via learning reachability estimators from rl policies. 2019. doi:10.48550/ARXIV.1907.04799. URL `https://arxiv.org/abs/1907.04799`.

[12] L. Janson and M. Pavone. Fast marching trees: a fast marching sampling-based method for optimal motion planning in many dimensions - extended version. *CoRR*, abs/1306.3532, 2013.

[13] J. Wang, W. Chi, C. Li, C. Wang, and M. Q.-H. Meng. Neural rrt*: Learning-based optimal path planning. *IEEE Transactions on Automation Science and Engineering*, 17(4):1748–1758, 2020.

[14]

[15] L.-C. Chen, G. Papandreou, F. Schroff, and H. Adam. Rethinking atrous convolution for semantic image segmentation, 2017. URL `https://arxiv.org/abs/1706.05587`.

[16] M. Bhardwaj. Motion planning dataset. `https://github.com/mohakbhardwaj/motion_planning_datasets`, 2017.

Appendix A: Maps

Map images

Appendix B: Execution Time vs Solution Cost

Plots

Appendix C: Execution Time vs Success Rate

Plots

Appendix D: Sample Count vs Collision Checks

Plots

Appendix E: Sample Count vs Success Rate

Plots

Appendix F: Comparison of Paths Found

Images

Appendix G: Group Contributions

Jazib Ahmad contributed...